Giant resonances in ^{24}Mg

D. H. Youngblood, Y.-W. Lui, and H. L. Clark

Cyclotron Institute, Texas A&M University, College Station, Texas 77843

The giant resonance region in ^{24}Mg was studied with inelastic scattering of 240 MeV α particles at small angles including 0°. The giant resonance peak was found to extend up to $E_X = 41$ MeV. Isoscalar $E0$, $E1$, and $E2$ strength corresponding to $72 \pm 10\%$, $81^{+26}_{-14}\%$, and $72 \pm 10\%$ of the respective energy weighted sum rules was identified in the peak with centroids of 21.0 ± 0.6, 18.8 ± 1.7, and 16.9 ± 0.6 MeV and rms widths of 7.3 ± 1.2, 6.7 ± 1.0, and 3.4 ± 0.5 MeV, respectively. Elastic scattering was measured from $\theta_{c.m.} = 3°$ to 33° and density dependent folding model parameters obtained. Inelastic scattering to states at 1.369, 4.122, 4.238, 6.010, 6.432, 7.349, 7.555, 7.616, and 8.358 MeV was measured and $B(EL)$ values obtained.
[S0556-2813(99)01607-6]

PACS number(s): 24.30.Cz, 25.55.Ci, 27.30.+t

INTRODUCTION

The isoscalar giant monopole resonance (GMR) is of interest because its energy is directly related to the compressibility of nuclear matter (K_{nm}) [1]. In the scaling approximation, nuclear compressibility is related [1] to $E_{GMR} = (m_3/m_1)^{1/2}$, where $m_k = \Sigma (E_n - E_0)^k |\langle 0|r^2|n\rangle|^2$. In order to account for contributions from finite nuclei and extract K_{nm}, macroscopic analyses [2] of the GMR require that the energy of the GMR be known in nuclei over a wide range of A. Lu *et al.* [3] in 1986 using inelastic scattering of 120 MeV α particles reported identification of $E0$ strength in ^{24}Mg corresponding to $90 \pm 20\%$ of the $E0$ energy-weighted sum rule (EWSR) between $E_X = 11-20$ MeV. In 1995 Dennert *et al.* [4] reported locating $97 \pm 25\%$ of the $E0$ EWSR in ^{24}Mg between $E_X = 10-23$ MeV using inelastic scattering of 156 MeV ^{6}Li ions. The data of Lu *et al.* did not extend above $E_X = 20$ MeV. In recent works [5,6] using inelastic scattering of 240 MeV α particles at 0° with a new spectrometer and beam analysis system, we obtained much higher peak to background ratios for quadrupole and monopole resonances than previous works. In ^{40}Ca [5] and ^{28}Si [6] we found evidence that the $E0$ strength extended up to and beyond $E_X = 30$ MeV which would make the reported $E0$ strength in ^{24}Mg unusually compact. Lu *et al.* also reported considerable isoscalar $E1$ strength between $E_X = 11-20$ MeV, and in ^{28}Si we found isoscalar $E1$ strength extending up to $E_X = 35$ MeV. Therefore we have studied ^{24}Mg beyond $E_X = 45$ MeV to identify high-lying giant resonance strength.

EXPERIMENTAL TECHNIQUE AND RESULTS

A beam of 240 MeV α particles from the Texas A&M K500 superconducting cyclotron bombarded self-supporting Mg foils enriched to 99.96% ^{24}Mg and located in the target chamber of the multipole-dipole-multipole spectrometer [7]. Beam was delivered to the spectrometer through a beam analysis system having two bends of 88° and 87° [8]. The beam was limited by slits after the first bend, and the second bend was used for clean up, with slits located so as not to intercept the primary beam. The horizontal acceptance of the spectrometer was 4° and ray tracing was used to reconstruct the scattering angle. The vertical acceptance was set at $\pm 2°$. When the spectrometer central angle (θ_{spec}) was set to 0°, the beam passed beside the detector and was stopped on a carbon block inside a Faraday cup behind the detector. For $3.5° < \theta_{spec} < 6°$, the beam was stopped on an insulated Ta block beside the solid angle defining slits. At larger angles the beam was stopped on a Faraday cup in the target chamber. At $\theta_{spec} = 0°$, runs with an empty target frame showed α particles uniformly distributed in position at a rate about 1/2000 of that with a target in place.

A 60 cm long focal plane detector covered approximately 55 MeV of excitation. Its principles of operation are similar to the detector described in Ref. [9]. It contains four proportional counters to measure *x*-position at four points along a rays path using the method of charge division, as well as an ionization chamber to provide ΔE and a scintillator to measure total energy and provide a fast timing signal for each ray. The out-of-plane scattering angle, ϕ, was not measured. To improve the quality of the position spectra, θ for each ray was calculated separately using data from independent wire pairs, and events in disagreement by more than two standard deviations were discarded [9]. Position resolution of approximately 0.9 mm and scattering angle resolution of about 0.09° were obtained. The angle calibration was obtained from an angle spectrum taken with a mask having five openings 0.1° wide spaced 1° apart. The actual spectrometer angle was determined from the kinematic crossover from the elastic scattering off hydrogen (in a ^{12}C target) and ^{12}C inelastic scattering peaks. The calibration procedures are described in detail in Refs. [9] and [10].

Data were also taken with ^{12}C and ^{28}Si targets at the actual field settings used in the experiments. The positions of the 9.641 and 18.350 MeV states [11] in ^{12}C, the 10.18, 18.67, and 20.43 MeV states [12] in ^{28}Si and the 12.86 and 17.36 MeV states [12] in ^{24}Mg were used to obtain momentum calibrations linear in position for each of the spectra. The energies of these known narrow peaks between 9 and 21 MeV were consistently reproduced better than 50 keV. Giant-resonance data were taken with the spectrometer central angle (θ_{spec}) set at 0°, 3.5°, 4.0°, and 5.5° covering the angular range from 0° to 7.5°. The excitation energy range observed was $7 < E_X < 60$ MeV. The effective energy resolu-
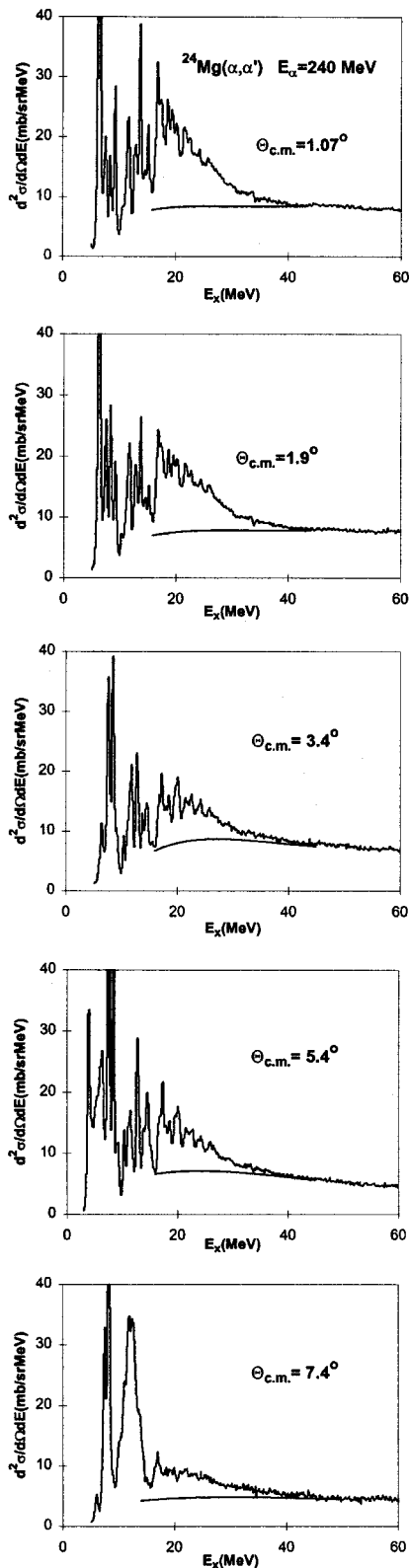
FIG. 1. Spectra obtained for ^{24}Mg(α,α') at $E_\alpha = 240$ MeV at five angles. The average center-of-mass angles are indicated. The top two were taken with the spectrometer at 0°, while the other spectra were taken with the spectrometer at 3.5° or 5.5°. The smooth line indicates the division between the continuum and the GR peak used for the analysis.
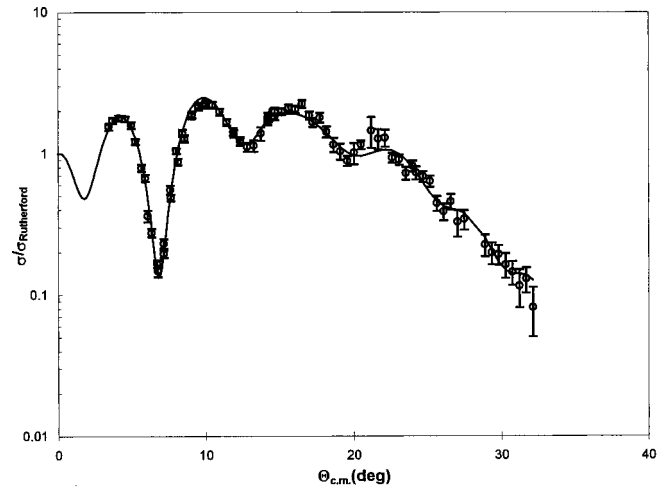

FIG. 2. Angular distribution of the ratio of the differential cross section for elastic scattering to Rutherford scattering for 240 MeV α particles from ^{24}Mg is plotted versus average center-of-mass angle. The solid line shows a DDWS calculation with the parameters from Table II.

tion was 250–300 keV. Sample spectra obtained are shown in Fig. 1.

Elastic and inelastic scattering data were taken at spectrometer angles of 3.5° and 5.5° at a higher dipole field setting covering the range $-10 < E_X < 45$ MeV but with the spectrometer acceptance the same as for the giant resonance data. In addition, elastic and inelastic scattering data were taken over the angle range from 2° to 30°, with the vertical acceptance of the spectrometer reduced to ±0.8°, in order to obtain optical-model parameters.

Each data set was divided into ten angle bins, each corresponding to $\Delta\theta \simeq 0.4°$ using the angle obtained from ray tracing. ϕ is not measured by the detector, so the average angle for each bin was obtained by integrating over the height of the solid angle defining slit and the width of the angle bin. For comparison with theoretical calculations, the data points are plotted at this average angle so that, for example, data from the central angle bin taken with the spectrometer at 0° would be plotted at $\theta_{lab} = 1.07°$. By plotting the data versus the average angle, the primary effect of the large solid angle is to fill in deep minima. The phase and cross section maxima are affected only slightly. With the reduced vertical opening [±0.8°], the cross section correction to the elastic scattering from averaging over the angle opening was 3% at 2.5° and less than 1% at larger angles except in the minima, when the averaged cross sections were plotted at the average angle determined as described above. This is particularly important for optical model fits because the optical model codes do not take into account averaging over a large vertical opening where the effective angular range for each data point is different.

Cross sections were obtained from the charge collected, target thickness, dead time and known solid angle. Two sets of data were taken in different experimental runs with targets of 2.81 mg/cm^2 (measured by weighing) and 4.41 mg/cm^2. The thickness of the 4.41 mg/cm^2 target was determined by measuring the position in the focal plane with the spectrom-
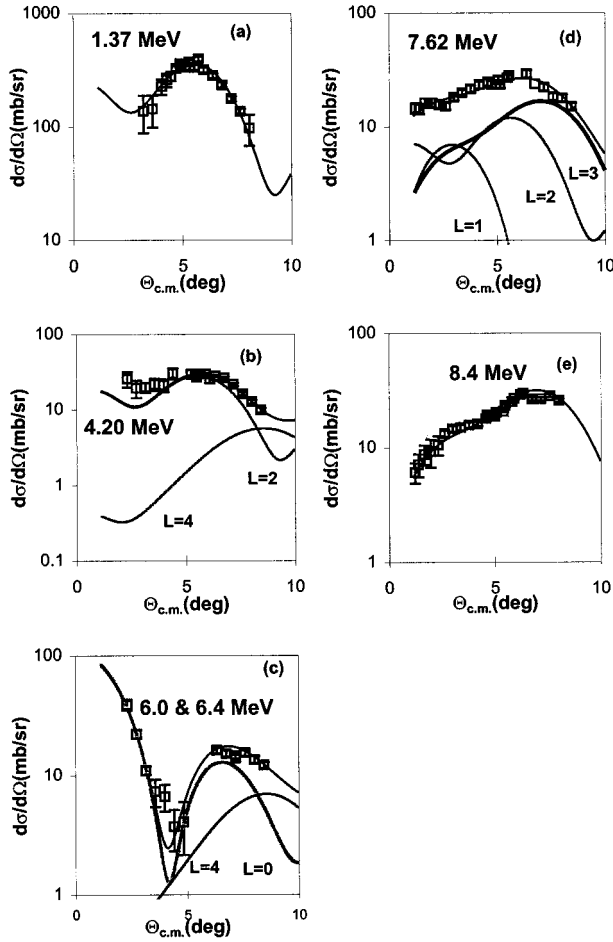
FIG. 4. Angular distributions of the differential cross section for inelastic α scattering for six excitation ranges in ^{24}Mg plotted versus average center-of-mass angle. The solid lines show the sum of the distributions for the individual multipolarities. The gray line shows the $L=0$ component, the dash-dot line shows the $L=2$ component, the dashed line shows the $L=1$ $T=0$ component, the wide black line shows the $L=3$ component, and the dash-dot-dot line shows the $L=4$ component for each of the regions. When not shown, errors are smaller than the data points.

FIG. 3. (a) Angular distribution of the differential cross section for inelastic alpha scattering to the 1.369 MeV 2^+ state in ^{24}Mg plotted versus average center-of-mass angle. The solid line shows an $L=2$ DDWS calculation for $B(E2)=0.045$ e^2fm^4. (b) Angular distribution of the differential cross section for inelastic alpha scattering to the 4.122 MeV 4^+ and 4.238 MeV 2^+ states in ^{24}Mg plotted versus average center-of-mass angle. The solid line shows a sum of $L=2$ and $L=4$ DDWS calculations for $B(EL)$ values in Table III. The $L=2$ ($L=4$) contribution is shown by the dash-dot (dash-dot-dot) line. (c) Angular distribution of the differential cross section for inelastic alpha scattering to the 6.010 MeV 4^+ and 6.432 MeV 0^+ states in ^{24}Mg plotted versus average center-of-mass angle. The solid line shows a sum of $L=0$ and $L=4$ DDWS calculations for $B(EL)$ values in Table III. The $L=0$ ($L=4$) contribution is shown by the gray (dash-dot-dot) line. (d) Angular distribution of the differential cross section for inelastic alpha scattering to the 7.349 MeV 2^+, 7.555 MeV 1^-, and 7.616 MeV 3^- states in ^{24}Mg plotted versus average center-of-mass angle. The solid line shows a sum of $L=1,2,3$ DDWS calculations for $B(EL)$ values in Table III. The $L=1,2,3$ contributions are shown by the dotted, dash-dot, wide black lines. (e) Angular distribution of the differential cross section for inelastic alpha scattering for a peak corresponding to $E_X=8.4$ MeV in ^{24}Mg plotted versus average center-of-mass angle. The solid line shows an $L=3$ DDWS calculation for $B(E3)=0.0025$ e^3fm^6.

eter at $0°$ of the 240 MeV α particle beam (intensity about 300 particles/second) with and without the target in place. The overall de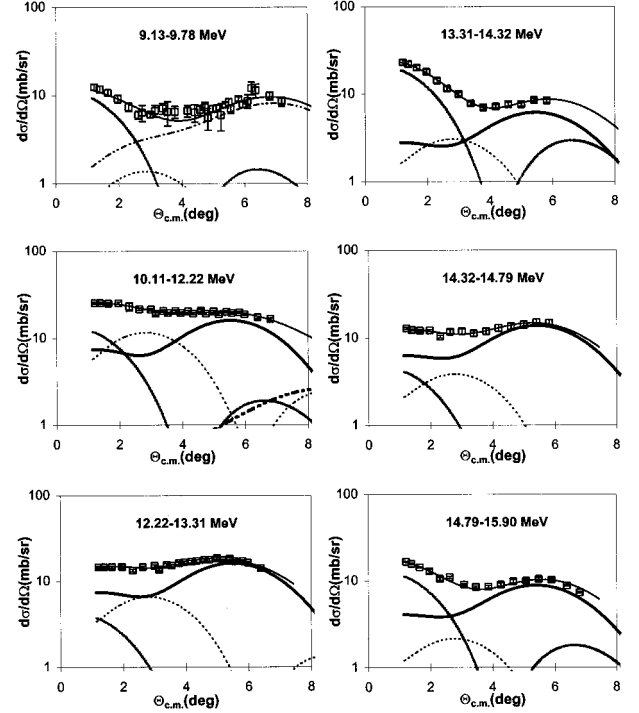ad time of the electronics and computer data acquisition system was measured by passing pulses from a random (in time) pulser into the preamplifiers and through the entire system into the computer. They were checked by comparing the total number of pulses sent to the computer with the number in the spectra. Dead times obtained from the two methods agreed to within 1%. Approximately 16% of events which made it into the computer were discarded because the angles measured in the two sets of horizontal wires did not agree. The cumulative uncertainties in target thickness, solid angle, etc. results in about a $\pm 10\%$ uncertainty in absolute cross sections. The consistency of the current integrator was checked with a monitor detector fixed at $20°$. Cross sections obtained from the two runs with different targets agreed to better than 5%.

Angular distributions of the elastic scattering and inelastic scattering exciting the 1.369 MeV 2^+ state, the 4.122 MeV 4^+ and 4.238 MeV 2^+ unresolved doublet, the 6.010 MeV 4^+ and 6.432 MeV 0^+ unresolved doublet, the 7.349 MeV 2^+, 7.555 MeV 1^-, and 7.616 MeV 3^- unresolved triplet and a group at 8.4 MeV (dominated by the 8.358 MeV 3^- state) are shown in Figs. 2 and 3, respectively. Cross sections obtained from the giant resonance and elastic scattering runs for the 7.6 and 8.4 MeV groups agreed within statistics.

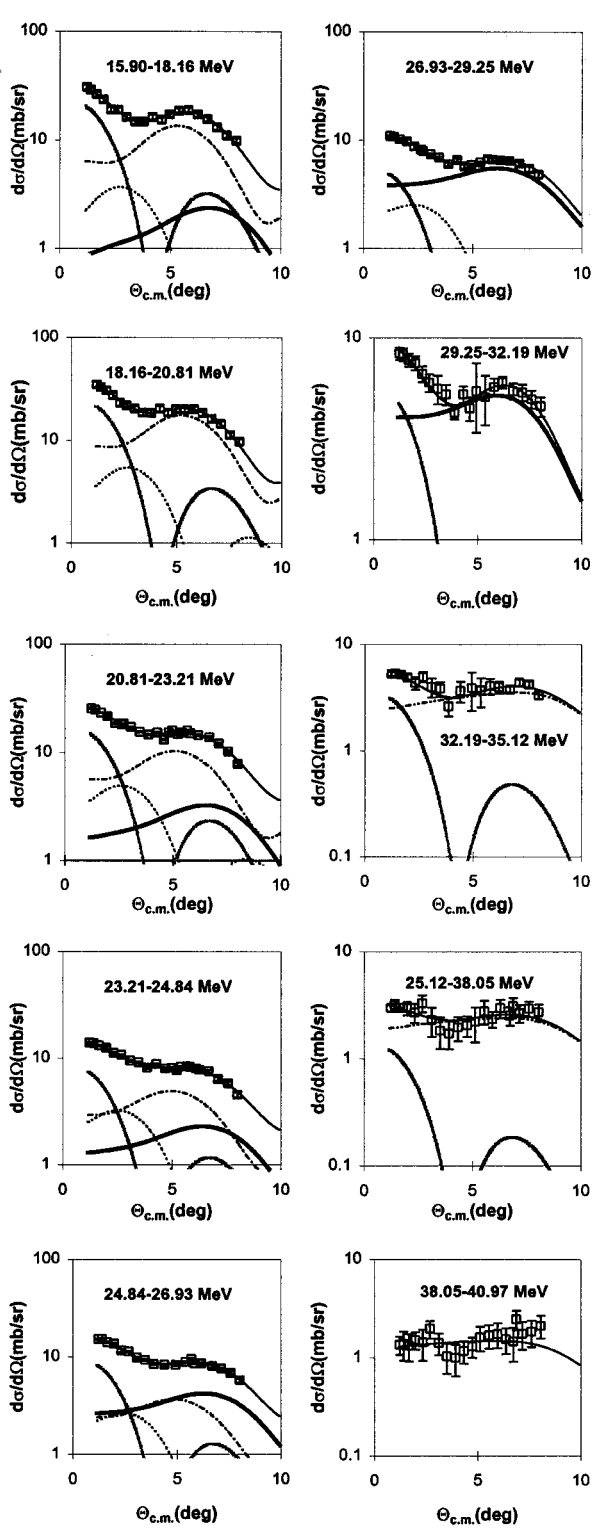The spectra in Fig. 1 (and earlier results from van der

FIG. 5. Angular distributions of the differential cross section for inelastic α scattering for ten excitation ranges of the giant resonance peak in ^{24}Mg plotted versus average center-of-mass angle. The solid lines show the sum of the distributions for the individual multipolarities. The gray line shows the $L=0$ component, the dash-dot line shows the $L=2$ component, the dashed line shows the $L=1$ $T=0$ component, the wide black line shows the $L=3$ component, and the dash-dot-dot line shows the $L=4$ component for each of the regions. When not shown, errors are smaller than the data points.
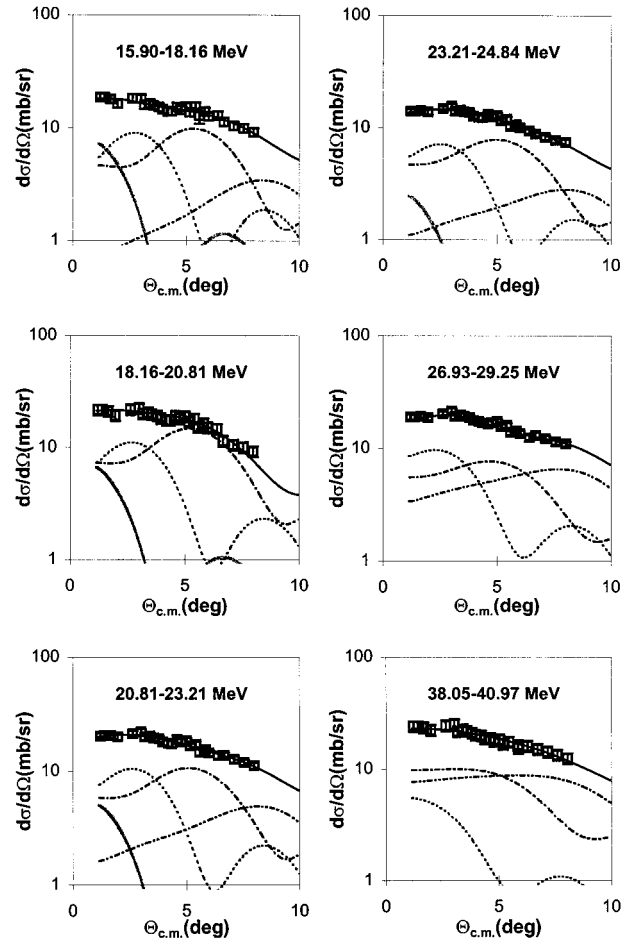

FIG. 6. Angular distributions of the differential cross section for inelastic α scattering for six excitation ranges of the continuum in ^{24}Mg plotted versus average center-of-mass angle. The solid lines show the sum of the distributions for the individual multipolarities. The gray line shows the $L=0$ component, the dash-dot line shows the $L=2$ component, the dashed line shows the $L=1$ $T=0$ component, and the dash-dot-dot line shows the $L=4$ component for each of the regions. When not shown, errors are smaller than the data points.

Borg *et al.* [12]) appear to show discrete states ending about $E_X=16$ MeV where a broad giant resonance peak (with structure) on a continuum begins. This peak appears to end at about $E_X=40$ MeV, considerably above the regions investigated in previous works. The apparent beginning of a continuum at about 16 MeV is consistent with the ^{23}Mg+n threshold (16.53 MeV). In the region from 9–16 MeV previous works have shown many states (the ^{20}Ne+α threshold is 9.31 MeV and the ^{23}Na+p threshold is 11.69 MeV) so we have not attempted to fit individual peaks above E_X =9 MeV. Instead the range $E_X=9-41$ MeV was broken into 16 excitation regions, each chosen roughly to correspond to visible structure in the spectra (unfortunately the structure changes with angle). At higher excitation where little structure is apparent, these regions were approximately 3 MeV wide. Above $E_X=15.9$ MeV the data were divided into a peak and a continuum (shown in Fig. 1) and these analyzed separately. As there is no experimental indication

TABLE I. Deformation lengths for 100% of the respective sum rules in ^{24}Mg.

Isoscalar	Deformation length (fm)	E_X (MeV)
$L=0$	$\alpha_0 c = 0.767$	18.0
$L=1$	$\beta_1 c = 0.433$	20.0
$L=2$	$\beta_2 c = 1.464$	18.0
$L=3$	$\beta_3 c = 2.337$	18.0
$L=4$	$\beta_4 c = 3.611$	18.0
Isovector		
$L=1$	$B(E1)=0.04455\, e^2\mathrm{b}$	20.0

TABLE II. Folding model parameters obtained from fits to elastic scattering.

V (MeV)	W (MeV)	R_i (fm)	a_i (fm)	R_c (fm)
41.02	35.39	4.176	0.614	3.835

of the beginning of a continuum at 15.9 MeV, the "continuum" chosen was obtained by smoothly connecting the spectra minima around $E_X = 9$ MeV to the region above $E_X = 45$ MeV. This results in a (non-physical) abrupt beginning of a continuum at $E_X = 15.9$ MeV so that clearly in the region of 16 MeV the continuum peak separation is arbitrary. Angular distributions obtained for the $E_X = 9$ to 16 MeV region are shown in Fig. 4, while those for the peak ($E_X = 16$ to 41 MeV) are shown in Fig. 5, and selected ones for the continuum are shown in Fig. 6.

DWBA AND OPTICAL MODEL ANALYSIS

The transition densities and sum rules for various multipolarities are described thoroughly by Satchler [13]. The GMR has generally been considered a breathing mode oscillation and the corresponding transition density is given by [13]

$$U = -\alpha_0 [3\rho + r\, d\rho/dr],$$

where for a state that exhausts the EWSR

$$\alpha_0^2 = 2\pi(\hbar^2/m)(A\langle r^2\rangle E_x)^{-1}.$$

The versions used for other multipoles in this work are given in Ref. [5].

Inelastic alpha scattering to collective states has been analyzed using either the deformed potential model or the folding model. Beene et al. [14] have shown that consistent agreement between electromagnetic transition strengths and those measured with light and heavy ion inelastic scattering for low lying 2^+ and 3^- states can only be obtained using the folding model. Satchler and Khoa [15], analyzing a 240 MeV α study of ^{58}Ni, compared results obtained using the deformed potential model, single folding using a Gaussian α-nucleon force with and without density dependence, and double folding using the BDM3Y1 nucleon-nucleon force which includes density dependence. Their conclusion was that each of the folding calculations gave very similar $0°$ cross sections for the GMR, and fit the data for the 4.475 MeV 3^- state using the electromagnetic $B(E3)$ value. In this study we extract $E0$, $E1$, $E2$ and (possibly) $E3$ strength, so we chose to do a density dependent single fold-

ing calculation with a Woods-Saxon imaginary term (DDWS) of the type described by Satchler and Khao [15].

Elastic and inelastic scattering folding model calculations were carried out with the code PTOLEMY [16]. The shapes of the real parts of the potentials and form factors for PTOLEMY were obtained using the codes SDOLFIN and DOLFIN [17]. The shapes (Woods-Saxon) of the imaginary part of the form factors were calculated externally and read into PTOLEMY for all L values. Input parameters for PTOLEMY were modified [18] to obtain a relativistic kinematically correct calculation. The amplitudes of the transition densities for the various multipoles obtained from the expressions in Ref. [5] for 100% of the respective sum rules are given in Table I. Radial moments for ^{24}Mg were obtained by numerical integration of the Fermi mass distribution assuming $c = 2.979$ fm and $a = 0.523$ [19].

Folding model parameters were obtained for ^{24}Mg by fitting the elastic scattering, and the resulting fit is shown in Fig. 2. The parameters obtained are listed in Table II. DDWS calculations were carried out for the states shown in Fig. 3 and are shown superimposed on the data. Except for the $E_X = 8.4$ MeV group, calculations for all states known to be present in a group were included and their strengths varied to minimize χ^2. The resulting $B(EL)$ values (%EWSR values for the 0^+ and 1^- states) are given in Table III. The 8.4 MeV group was fit well by $L=3$ alone, though states with other multipolarities should be excited. For comparison $B(EL)$ values obtained from the NNDC compilation [20] of gamma decay data and from compilations of measured $B(EL)$ values [21,22] for the 1.369 and 7.616 MeV states are given. Except for the $E_X = 4.238$ MeV state where our result is somewhat high, the $B(EL)$ values obtained agree with electromagnetic values within the errors. The breathing mode transition density was used for the calculation for the 6.4 MeV $L=0$ state, and the $E0$ EWSR fraction obtained ($5.6\% \pm 1.0\%$) is in agreement with electron scattering [$6.3\% \pm 0.4\%$], where the Helm model was used [23]. It is also in agreement with the 5.4% obtained by van der Borg et al. [12] in a study of ^{24}Mg with 120 MeV α scattering. The 120 MeV data of van der Borg et al. [12] were analyzed with the deformed potential model which has been shown in several cases [5,15] to give $E0$ cross sections in agreement with the folding model. However, for $L \geq 2$ it has been shown [14] to deviate considerably from electromagnetic values, so we have not compared our results to deformed potential analyses for the other states. While the 6.4 MeV state was observed in the inelastic scattering data, it was at the edge of the detector where the effective acceptance is changing rapidly, so a reliable cross section could not be extracted. The data shown were obtained from the elastic scattering spectra taken at spectrometer angles of $3.5°$ and

TABLE III. $B(EL)$ values obtained for low-lying states in ^{24}Mg.

E_x (MeV)	J^π	$B(EL)_{EM}$[a] $(e'\,\mathrm{fm}^{2\ell})$	$B(EL)^e$ $(e'\,\mathrm{fm}^{2\ell})$	$B(EL)$ (this work) $(e'\,\mathrm{fm}^{2\ell})$
1.369	2^+	0.0435 ± 10	0.0432 ± 12[e]	0.045 ± 5
4.122	4^+			0.00018^{+3}_{-8}
4.238	2^+	0.0332 ± 20		0.044^{+10}_{-3}
6.010	4^+	0.00042 ± 10[c]		0.00023^{+7}_{-10}
		0.00036 ± 10[d]		
6.432	0^+	$6.3 \pm 0.4\%$[b,c]		$5.6 \pm 1.0\%$[b]
7.349	2^+	0.00118 ± 51		0.0015^{+8}_{-2}
7.555	1^-			$3 \pm 1\%$[b]
7.616	3^-	0.00150 ± 30	0.00112 ± 22[f]	0.0011^{+2}_{-3}
8.358	3^-	0.0031 ± 10		0.0025 ± 4

[a]Reference [20].
[b]% EWSR.
[c]Reference [23] Helm model.
[d]Reference [23] Tassie model.
[e]Reference [21].
[f]Reference [22].

5.5°. The statistics in the 6.0–6.4 MeV group were too small to reliably separate the peaks, so the cross section for the group was obtained.

DISCUSSION

Fits to the angular distributions shown in Figs. 4–6 were carried out with a sum of isoscalar $0^+, 1^-, 2^+, 3^-$, and at higher excitation, 4^+ strengths. The isovector giant dipole (IVGDR) cross section would be negligible and was not added in. The strengths were varied to minimize χ^2. The errors in strengths were estimated by changing the magnitude of the strength of one component until refitting by varying the other components resulted in a χ^2 twice that of the best fit. Monopole strength is characterized by strong peaking of the cross section at 0°. Thus $E0$ strength can be identified by strong forward peaking in the angular distribution. The IVGDR is also forward peaked (excited only by Coulomb excitation in ^{24}Mg), but is much weaker than the other multipolarities and has no impact on this analysis. The isoscalar $E1$ angular distributions peak around 3° and primarily fill in the valley in the angular distributions, particularly when $E0$ strength is present. Thus the extracted isoscalar $E1$ strength is probably the least definite and this is reflected in the uncertainties assigned. Over the angle range of the data, angular distributions for $L \geq 3$ are similar and small components of $L=3$ could not be distinguished from small components of $L=4$. At higher excitation energies, however, the cross section is falling slowly or increasing for $\theta \geq 7°$ and this behavior could not be fit with $L < 4$. The fits obtained along with the individual components of the fits are shown superimposed on the data in Figs. 4–6. DDWS calculations were carried out for each energy interval, and the change in angular distribution shapes with E_X can be seen in the figures.

The $E0$, $E1$, $E2$, and $E3$ strength distributions and errors obtained from the data (excluding the continuum above $E_X = 15.9$ MeV except for $E0$ strength) are shown in Fig. 7. The $E0$, $E1$, $E2$ and $E4$ strengths obtained for the continuum are shown in Fig. 8. The continuum angular distributions are similar over the entire energy range and can be fit primarily by a sum of $E1$, $E2$, and $E4$ angular distributions with small amounts of $E0$ strength below $E_X = 28$ MeV. The $E0$ strength extracted from the continuum data represents $10 \pm 4\%$ of the $E0$ EWSR. The strengths of the other multipoles required to fit the continuum increase almost monotonically up to the highest excitation observed and for $E1(500\%)$ and $E2(160\%)$ significantly exceed the sum rule. Clearly reaction mechanisms other than multipole transitions are responsible for a significant part of the continuum and thus higher multipole components cannot be extracted from the continuum in this manner. The multipole distributions for regions above $E_X = 16$ MeV shown in Fig. 7 include contributions only from the peak for $E1$, $E2$, and $E3$, however the $E0$ component from the continuum is included because its behavior in the continuum (small and dying off above 28 MeV) is consistent with a small error in drawing the continuum. The sum rule strengths and energy moments for the distributions shown in Fig. 7 are given in Table IV. The uncertainties given are those obtained from the fits and include uncertainties in the cross section. Uncertainties due to the separation of the peak and continuum (above $E_X = 16$ MeV) are not included and particularly for $E1$ and $E2$ strength could be substantial.

Since monopole strength is strongly forward peaked, a "spectrum of $E0$ cross section" was also generated by subtracting spectra taken at larger angles from those taken at the smallest angles [5,24]. This was converted to $E0$ strength and is shown in Fig. 9(a) along with the $E0$ strength extracted from the fits to the angular distributions. They are generally in good agreement. The large fluctuations in $E0$ strength in the subtracted spectrum at high excitation are due
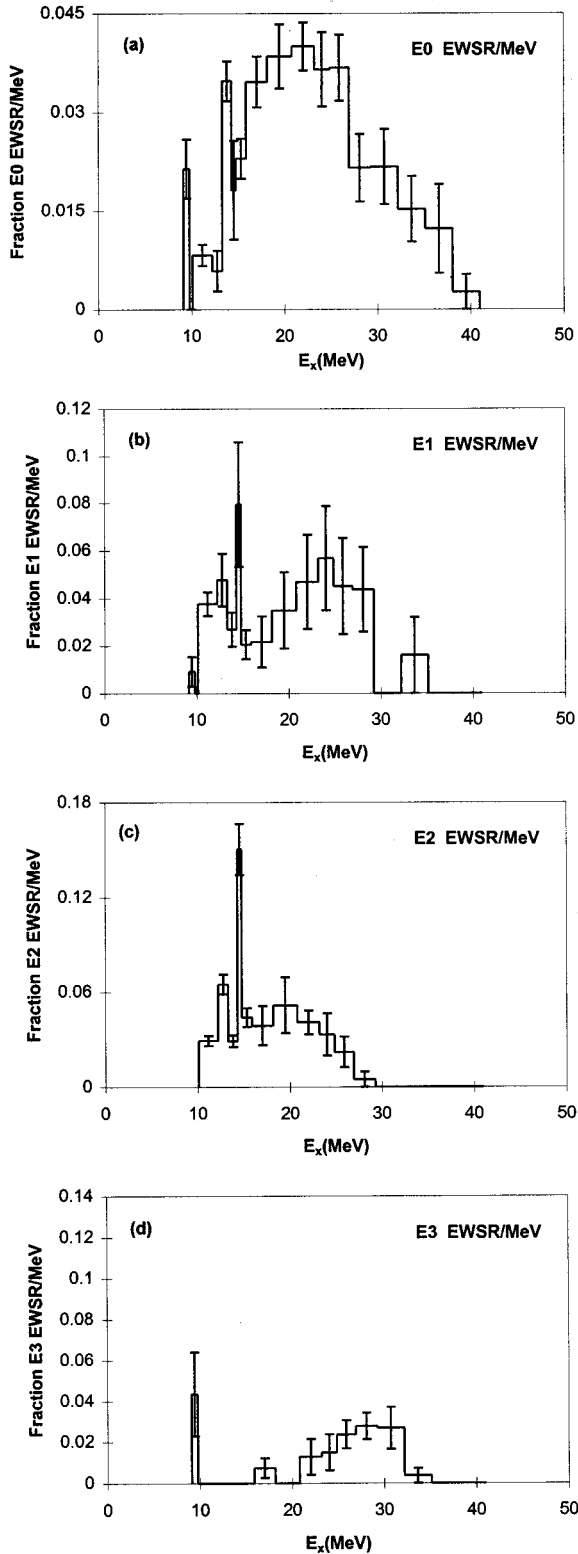
FIG. 7. (a)–(d) The solid lines show the fractions of the isoscalar EWSR in ^{24}Mg obtained in this work for the multipolarities indicated. The error bars represent the uncertainty due to the fitting of the angular distributions.

to statistical fluctuations in the subtracted spectrum. At high excitation, small cross sections correspond to large $E0$ strength [5,6]. The $E0$ strength above $E_X=9$ MeV in the
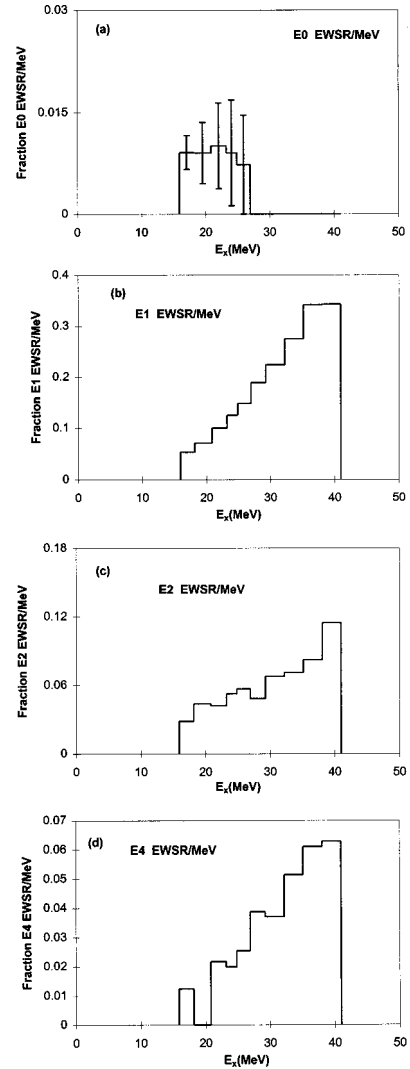

FIG. 8. (a) The solid line shows the fraction of the $E0$ EWSR in ^{24}Mg obtained from the fits to the angular distributions of the continuum. The error bars represent the uncertainty due to the fitting of the angular distributions. (b)–(d) The solid line shows the fraction of the isoscalar EWSR obtained for the multipolarity indicated from the fits to the angular distributions of the continuum.

subtracted spectrum corresponds to $76\pm15\%$ of the $E0$ EWSR, where the uncertainty is due to the uncertainty of the angle bin width of the two spectra [5,6], in excellent agreement with the 72% obtained from the fits. The centroid

TABLE IV. Sum rule strengths and energy moments obtained for the distributions shown in Fig. 7 for the excitation range E_x 9–41 MeV.

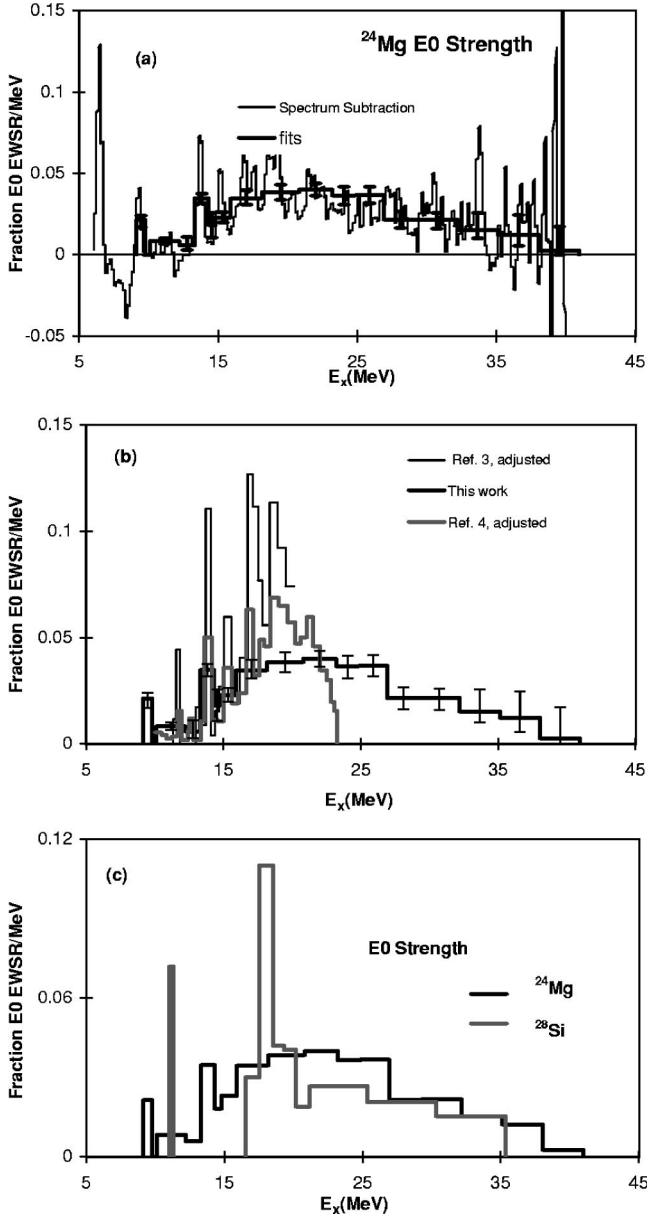| L	%EWSR	m_1/m_0 (MeV)	rms width (MeV)
0	72 ± 10	21.0 ± 0.6	7.3 ± 1.2
1	81^{+26}_{-14}	18.8 ± 1.7	6.7 ± 1.0
2	72 ± 10	16.9 ± 0.6	3.4 ± 0.6
3	31^{+9}_{-6}	25.2 ± 1.0	4.5 ± 1.2

FIG. 9. (a) The thicker dark line shows the fraction of the $E0$ EWSR obtained from fits to the angular distributions. The thin dark line shows the fraction of the $E0$ EWSR obtained from the difference spectrum as described in the text. (b) The thick dark line shows the $E0$ strength obtained in this work. The gray line shows the (adjusted, see text) $E0$ strength from Ref. [4] and the thin dark line shows the (adjusted, see text) $E0$ strength from Ref. [3]. (c) The thick dark line shows ^{24}Mg $E0$ strength and the gray line shows ^{28}Si $E0$ strength [6].

(m_1/m_0) obtained from the subtracted spectrum is 22.7 ± 1.3 MeV, in agreement with the 21.0 ± 0.6 MeV obtained from the angular distributions. Energy calibration errors are small compared to the contributions from the errors in strength, and contribute around 100 keV (in quadrature) to the error.

The present work is compared to the studies of Lu *et al.* [3] in Table V. For the region $E_X = 11-20$ MeV the $E1$ and $E2$ strengths obtained in the two experiments agree within

TABLE V. Comparison of present GR results with other work. (*) See text.

E_x (MeV)	J^π	This work %EWSR	Ref. [3] %EWSR	Ref. [3] adjusted* %EWSR
11–20	0^+	37 ± 5	90 ± 20	46 ± 15
11–20	1^-	37 ± 12	56 ± 12	
11–20	2^+	51 ± 16	51 ± 11	40 ± 14
			Ref. [4]	Ref. [4] adjusted*
10–23.5	0^+	45 ± 7	97 ± 25	45 ± 8

the errors, however Lu *et al.* report $90\% \pm 20\%$ whereas we identify only $37\% \pm 5\%$ of the $E0$ EWSR in this region. We did DWBA calculations for some of the data reported by Lu *et al.* [3] and van der Borg *et al.* [12], using optical potentials from van der Borg *et al.* [12]. Lu *et al.* reference van der Borg *et al.* for the optical parameters used for their analysis. Neither gave the Fermi parameters used for the sum rule calculations, so we used the Fermi parameters given above. The strengths determined by comparing our calculations to their data are shown in Table VI and for $L=2$ have been corrected by the factor of 1.24 given by van der Borg *et al.* [12]. For the 1.369 MeV 2^+ and 6.432 MeV 0^+ states our results agreed with those of van der Borg *et al.* (within 2% and 10%, respectively) within the errors of determining the data values from their graphs. For the 12.09 MeV 2^+ strength we obtain an $E2$ EWSR about 83% of that obtained by Lu *et al.* which is probably within the accuracy with which the graph can be read. However, for the 11.67 and 18.0 MeV 0^+ data shown by Lu *et al.* we obtain $E0$ EWSR fractions approximately half (49% and 53%) those quoted by Lu *et al.* Reducing Lu *et al.*'s total $E0$ strength by this factor would result in $46\% \pm 15\%$ of the $E0$ EWSR between $E_X = 11-20$ MeV from the Lu *et al.* data compared with $37\% \pm 5\%$ over this energy range in the present work.

Dennert *et al.* [4] reported $97\pm25\%$ of the $E0$ EWSR in the region $E_X = 10-23$ MeV whereas for that region we obtain $45\pm7\%$ of the $E0$ EWSR (Table V). They have used a nonconventional normalization of the DWBA to the angular distributions (their Fig. 3), however. The peak of the data for the $L=0$ strength (at about $1°$) is about a factor of 2 below the peak of the DWBA. This results in an $E0$ strength about a factor of 2 higher than if they had normalized to the peak,

TABLE VI. Comparison of EWSR results from our DWBA calculations and those of the original authors for the ^{24}Mg data of Refs. [3] and [12].

E_x (MeV)	J^π	Our calculation %EWSR	Ref. [3] %EWSR	Ref. [12] %EWSR	Ratio
1.37	2^+	12		11.7	1.0
6.43	0^+	4.9		5.4	0.91
12.09	2^+	0.9	1.1		0.83
11.67	0^+	0.89	1.8		0.49
18.0	0^+	3.0	5.6		0.53

as is normally done. Graphically adjusting their calculations to fit their data requires about a factor of 2.1, so that their ''adjusted'' $E0$ strength would be $45\pm12\%$ for this region, in excellent agreement with the 45% obtained in this work. The $E0$ distributions of Lu *et al.* and Dennert *et al.*, after adjustment as described, are compared to this work in Fig. 9(b).

While the data of Lu *et al.* [3] ended at $E_X=20$ MeV, that of Dennert *et al.* [4] continued to nearly $E_X=30$ MeV, and using the ''subtraction of spectra'' technique [5,24] they reported that there was no excess strength above $E_X=23$ MeV leading to the conclusion that the $E0$ strength ended there. Our results suggest that between $E_X=23-30$ MeV there may have been other processes present in their data that increased with angle, canceling the relatively small contributions from the $E0$ strength in that region. This could have been aggravated by the relatively small statistics in their data, apparent from the statistical fluctuations in the spectra they show.

The $E0$ strength distributions obtained for ^{28}Si [6] and for ^{24}Mg are shown in Fig. 9(c). At lower excitation large differences in structure are apparent, however the distributions are similar above $E_X=20$ MeV, except that the ^{28}Si strength ends at $E_x=35$ MeV whereas the ^{24}Mg strength extends up to $E_X=39$ MeV. This may be an artifact of the analysis because the statistics obtained for the ^{24}Mg data were considerably better (about six times the number of counts) which is very important in determining the separation of the giant resonance peak and the continuum at high excitation.

CONCLUSIONS

In this work we have shown that the giant resonance peak in ^{24}Mg extends up to about $E_X=41$ MeV consistent with our earlier results for ^{28}Si (35 MeV) and ^{40}Ca (>30 MeV) rather than ending around 20–23 MeV as suggested in earlier

works [3,4]. We have identified $72\pm10\%$ of the $E0$ EWSR in this region with a centroid 21.0 ± 0.6 MeV, considerably higher than the approximately 18 MeV reported in earlier works. The strength is broad with an rms width of 7.3 MeV (Gaussian FWHM equivalent 17.5 MeV). The $E1$, $E2$, and $E3$ (or $L\geq=3$) strength in the giant resonance peak also continues at higher excitation than previous reports, ending just below 30 MeV for $E2$, and at about 35 MeV for $E1$ and $E3$. Above $E_X=35$ MeV, $E4$ (and $E0$) strength is required to fit the angular distributions. The presence of substantial $E0$ strength above $E_X=23$ MeV conflicts with earlier reports of 90% and 97% of the $E0$ EWSR in a moderately compact GMR in ^{24}Mg. If we accept either Lu *et al.*'s or Dennert *et al.*'s normalization then our work would have identified over 150% of the $E0$ EWSR in ^{24}Mg. As 500% of the isoscalar $E1$ sum rule and 150% of the $E2$ sum rule would be required to fit the continuum (above $E_X=16$ MeV) if it consists only of multipole transitions, there clearly are processes other than multipole excitation present at higher excitation in the continuum.

The centroids of $E0$ strength in ^{24}Mg(21.0 MeV) and ^{28}Si(20.8 MeV) are now in excellent agreement, however this work suggests that not all of the strength has yet been located in either nucleus and hence these centroids cannot be used in the Leptodermous expansion [1,2] to extract nuclear matter incompressibility. In a recent work [25] we compared the energies of the GMR in heavier nuclei to microscopic calculations with the Gogny interaction to conclude that $K_{nm}=231\pm5$ MeV and this is perhaps the most reliable method to determine K_{nm}.

[1] J. P. Blaizot, Phys. Rep. **64**, 171 (1980).

[2] S. Shlomo and D. H. Youngblood, Phys. Rev. C **47**, 529 (1993).

[3] H. J. Lu, S. Brandenburg, R. De Leo, M. N. Harakeh, T. D. Poelhekken, and A. van der Woude, Phys. Rev. C **33**, 1116 (1986).

[4] H. Dennert, E. Aschenauer, W. Eyrich, A. Lehmann, M. Moosburger, N. Scholz, H. Wirth, H. J. Gils, H. Rebel, and S. Zagromski, Phys. Rev. C **52**, 3195 (1995).

[5] D. H. Youngblood, Y.-W. Lui, and H. L. Clark, Phys. Rev. C **55**, 2811 (1997).

[6] D. H. Youngblood, H. L. Clark, and Y.-W. Lui, Phys. Rev. C **57**, 1134 (1998).

[7] D. M. Pringle, W. N. Catford, J. S. Winfield, D. G. Lewis, N. A. Jelley, K. W. Allen, and J. H. Coupland, Nucl. Instrum. Methods Phys. Res. A **245**, 230 (1986).

[8] D. H. Youngblood and J. D. Bronson, Nucl. Instrum. Methods Phys. Res. A **361**, 37 (1995).

[9] D. H. Youngblood, Y.-W. Lui, H. L. Clark, P. Oliver, and G. Simler, Nucl. Instrum. Methods Phys. Res. A **361**, 539 (1995).

[10] H. L. Clark, Y.-W. Lui, and D. H. Youngblood, Nucl. Phys. **A589**, 416 (1995).

[11] F. Ajzenberg-Selove, Nucl. Phys. **A506**, 1 (1990).

[12] K. van der Borg, M. N. Harakeh, and A. van der Woude, Nucl. Phys. **A365**, 243 (1981).

[13] G. R. Satchler, Nucl. Phys. **A472**, 215 (1987).

[14] J. R. Beene, D. J. Horen, and G. R. Satchler, Phys. Lett. B **344**, 67 (1995).

[15] G. R. Satchler and Dao T. Khoa, Phys. Rev. C **55**, 285 (1997).

[16] M. Rhoades-Brown, M. H. Macfarlane, and S. C. Pieper, Phys. Rev. C **21**, 2417 (1980); M. H. Macfarlane and S. C. Pieper, Argonne National Laboratory Report No. ANL-76-11, Rev. 1, 1978 (unpublished).

[17] L. D. Rickerston, the folding program DOLFIN, 1976 (unpublished).

[18] G. R. Satchler, Nucl. Phys. **A540**, 533 (1992).

[19] G. Fricke, C. Bernhardt, K. Heilig, L. A. Schaller, L. Schellenberg, E. B. Shera, and C. W. DeJager, At. Data Nucl. Data Tables **60**, 177 (1995).

[20] P. M. Endt, Nucl. Phys. **A251**, 1 (1990). Data extracted from the ENSDF database, version (90), NNDC.

[21] S. Raman, C. H. Malarkey, W. T. Milner, C. W. Nestor, Jr., and P. H. Stelson, At. Data Nucl. Data Tables **36**, 1 (1987).

[22] R. H. Spear, At. Data Nucl. Data Tables **42**, 55 (1989).

[23] A. Johnston and T. Drake, J. Phys. A **7**, 898 (1974).

[24] S. Brandenburg, R. De Leo, A. G. Drentje, M. N. Harakeh, H. Sakai, and A. van der Woude, Phys. Lett. **130B**, 9 (1983).

[25] D. H. Youngblood, H. L. Clark, and Y.-W. Lui, Phys. Rev. Lett. **82**, 691 (1999).